### 5.2 Deep event

Our second simulation is for the 1994 June 9 deep Bolivia event of magnitude $M_w = 8.2$. The focal mechanism is illustrated in Fig. 11; the depth is 647 km. We use a moment-rate function similar to the one used for the Irian Jaya event (Fig. 12), but with a slightly shorter half-duration of 15 s.

At this point we wish to validate our implementation of attenuation in the method. Associated with PREM is a five-layer attenuation model. As mentioned earlier, we only incorporate shear attenuation: bulk attenuation can be safely neglected because the bulk Q is several hundred times larger than the shear Q. The calculation of normal-mode seismograms for anelastic Earth models is based upon first-order perturbation theory, which is acceptable for the attenuation associated with PREM (e.g. Dahlen & Tromp 1998); however as a consequence the mode synthetics in this section are not as accurate as in the purely elastic case of the previous section. For each layer we determine stress and stain relaxation times $\tau_\ell^\sigma$ and $\tau_\ell^\epsilon$ for an absorption-band model over the period range between 20 and 1000 s, based upon three standard linear solids. Because of

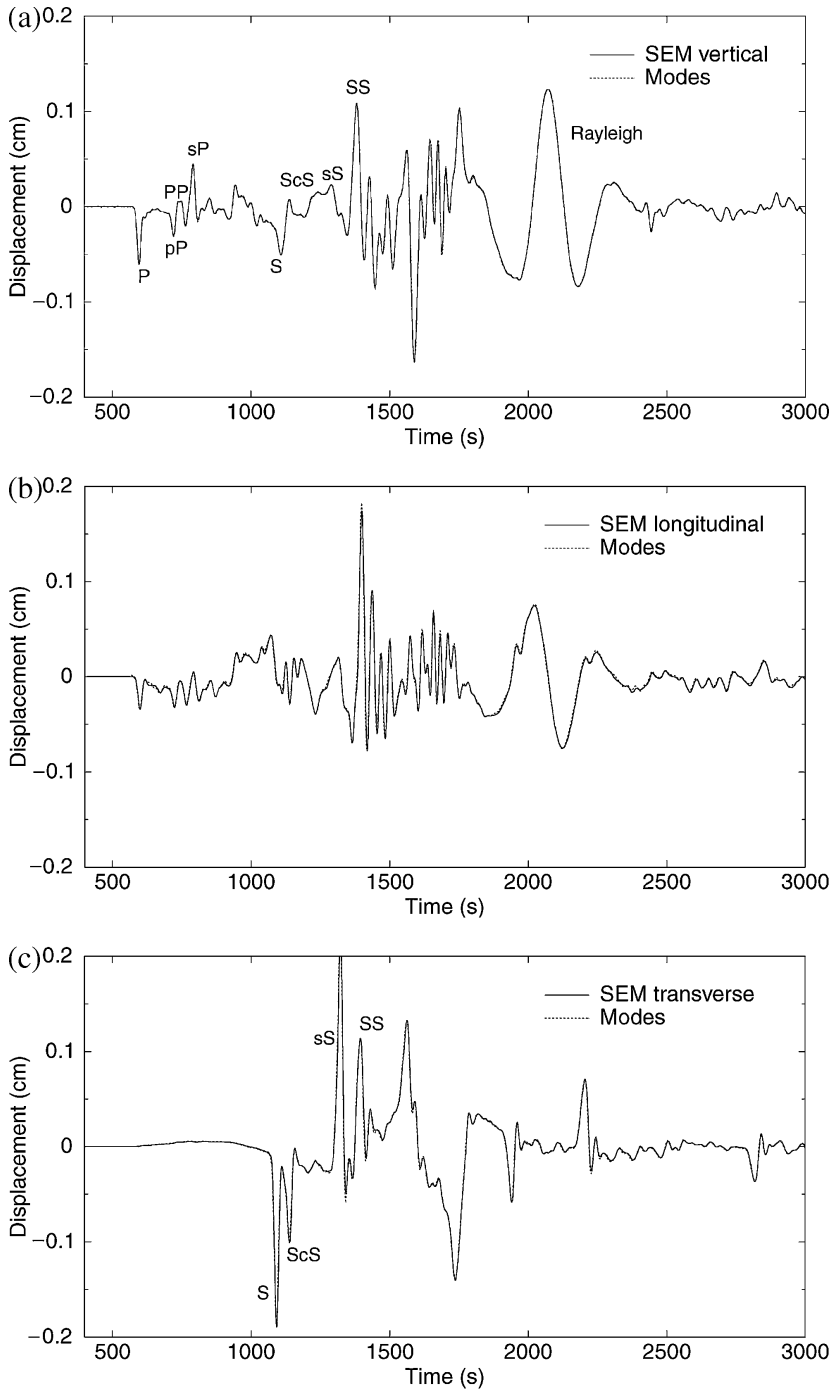


**Figure 21.** SEM (solid line) and mode (dotted line) synthetic seismograms for the great magnitude 8.2 1994 June 9 Bolivia earthquake, recorded at TriNet station PAS in Pasadena, California. The depth of the event is 647 km. Anisotropy and attenuation are both included in this simulation. (a) Vertical component, (b) longitudinal component, (c) transverse component. The agreement is almost perfect on the three components.

the broad period range, a solution based upon two solids does not give a satisfactory result. We evenly space the three stress relaxation times $\tau_\ell^\sigma$ in logarithmic frequency. Next, we determine the strain relaxation times $\tau_\ell^\epsilon$ by minimizing the difference between the desired constant Q and predictions based upon the series of three standard linear solids using a simple iterative inversion scheme. Table 1 summarizes the stress and strain relaxation times used to reproduce the appropriate PREM Q values. Fig. 19 illustrates that the series of three standard linear solids can approximate a constant Q efficiently to within a few per cent. Associated with the absorption-band model is physical dispersion which affects the arrival times of the waves. To accommodate this, we take PREM, which has a reference frequency of 1 Hz, i.e. $\omega_0 = 2\pi$, and determine the shear modulus appropriate for a frequency $\omega_c$ at the logarithmic centre of the frequency range of interest (Liu *et al.* 1976):

$$\mu(\omega_c) = \mu(\omega_0)\,[1 + 2/(\pi\, Q_\mu)\ln(\omega_c/\omega_0)]. \qquad (49)$$

Given $\mu(\omega_c)$ we can calculate the relaxed modulus $\mu_R$, from which we obtain the time dependent modulus $\mu(t)$ and the unrelaxed modulus $\mu_U$ based upon eqs (8) and (10), respectively. Fig. 19 also illustrates that, over the frequency band of interest, the dispersion associated with the PREM Q model is very well mimicked by three standard linear solids.

In Fig. 20 we compare normal-mode and SEM synthetics at station ST04 of the BANJO array in Bolivia at a distance of 5° south of the epicentre (more details about the BANJO array can be found in Clarke *et al.* 1995). This simulation is motivated by an experiment performed by Ekström (1995) who used normal-mode summation to analyze the static offset resulting from the event, and by the observations of a large offset in the BANJO data by Jiao *et al.* (1995). Again we find very good agreement between the modes and the SEM. In particular, the strong near-field term linking the *P* and *S* arrivals is accurately modelled, and the static offset of 6.6 mm on the vertical component and 7.3 mm on the North–South component is well recovered. Note also the distinct *ScS* arrival on this component at 800 s and the *sScS* arrival at 1080 s, which are perfectly reproduced. These *ScS* phases are clearly observed in the BANJO data (Clarke *et al.* 1995).

Next, we check the results of our simulation at teleseismic distance at the Pasadena, California, TriNet station PAS at an epicentral distance of 68°. Fig. 21 shows the three components of displacement both for the modes and the SEM. To appreciate the effects of attenuation and how accurately it has been modelled by the SEM, we show in Fig. 22 the vertical component of displacement computed using modes with and without attenuation. One can see that the waveforms are significantly affected by attenuation, both in phase and amplitude. In Fig. 23 we compare our SEM synthetic seismogram for the vertical component of velocity at PAS to the real data. Both records have been lowpass-filtered with the same six-pole two-pass Butterworth filter with a corner period of 40 s, and our synthetics have been convolved with the instrument response. We note that this is the only time in this study that we filter our synthetics. The agreement is quite satisfactory, keeping in mind that our synthetics are based upon PREM and therefore do not include effects due to 3-D heterogeneity.

To illustrate that our implementation of the inner core is correct, we show in Fig. 24 a close-up of *PKP* arrivals on the vertical component. The *PKP* waveforms are very sensitive to the very high value of Poisson's ratio, 0.44, in the inner core: if the shear-wave velocity is not correctly represented, the *PKP* waveforms change considerably. Numerically this poses a challenge, because if the mesh is not fine enough the very slow inner-core shear-wave velocity of about 3.6 km s$^{-1}$ is not sampled by enough points per wavelength. In our results, the *PKP*(AB) and *PKP*(BC) outer core branches as well as the *PKP*(DF) inner core branch are all very accurately modelled. A very weak $P_{\rm diff}$ arrival can be seen in the P shadow in both synthetics. The *PKP*(DF) arrival has travelled through the cube at the centre of the inner core, which is handled by one processor that needs to interact with all the other processors in the parallel implementation of the method, as explained previously. Note the very prominent depth phases, e.g. *pPKP*(DF), which arrive about two and a half minutes after the corresponding direct phases due to the large depth of the event. To appreciate the level of accuracy involved in the calculation of the *PKP* phases, note from Fig. 18 that the amplitudes of these arrivals are tiny compared to the later parts of the record (the depth of the event does not significantly affect this observation).

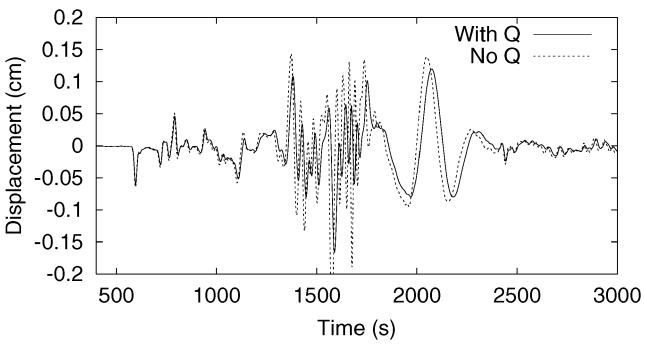


**Figure 22.** To illustrate the effects of attenuation and physical dispersion associated with anelastic PREM, we compare vertical component mode synthetics for PREM with (solid line) and without (dotted line) incorporating the effects of anelasticity. Note that elastic PREM is faster than anelastic PREM, and that in particular the S wave is significantly attenuated.

## 6 CONCLUSIONS

We have developed and implemented a spectral-element method (SEM) for the simulation of global seismic wave propagation. The method has been carefully benchmarked against normal-mode synthetics for elastic and anelastic versions of spherically symmetric earth model PREM. The SEM accurately incorporates effects due to the slow, thin crust, a transversely isotropic asthenosphere, sharp

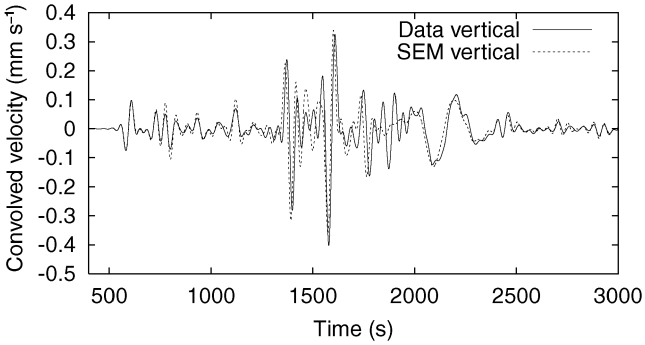


**Figure 23.** Comparison between SEM synthetics for anelastic, anisotropic PREM and real data recorded at TriNet station PAS in Pasadena, California, after the 1994 June 9 Bolivia event. Both vertical component velocity records have been lowpass-filtered with the same six-pole two-pass Butterworth filter with a corner period of 40 s, and the SEM synthetics have been convolved with the instrument response. This is the only time in this study that we filter SEM synthetics.